INSTITUT FÜR AERODYNAMIK
UND GASDYNAMIK

Direktor: Prof. Dr.-Ing. F. X. Wortmann
UNIVERSITÄT STUTTGART

AIRFOIL PROFILES FOR WIND TURBINES

F.X. WORTMANN

This report has been prepared in fulfilment of the research contract
"Investigation of rotor stressing and smoothness of operation of large-scale wind energy conversion systems",
sponsored by the International Energy Agency
with participation of the BMFT (ET 4086 A).
(Implementing agreement for a programme of research and development on wind energy conversion systems, annex IV)

Institute-Report 78-9
Stuttgart 1978

Airfoil profiles for wind turbines

by

F.X. Wortmann [+)]

In the following the requirements of wind turbine airfoils are briefly considered and a report is given of the design of some suitable airfoils together with results of test measurements at moderate and large angles of attack. The report concludes with a few observations about rough airfoils, pitch coefficients as well as allowable degrees of roughness and the avoidance of roughnesses due to insects.

1. Requirements

The blades of wind turbines with high tip speed ratio have a very high slenderness ratio. Their absolute torsional stiffness is therefore limited in the same way as for a helicopter blade. In order to shift the limit of static instability (blade static divergence) as well as the limit of flutter to as high speeds as possible, the airfoils - at least in the outer section of the blade - should have a more or less fixed centre of pressure.

At the same time the outer sections of the blades should possess the best lift/drag ratios that are possible over a relatively wide lift range. The lift values with low drag should cover approximately the range $0.5 < c_l < 1.5$, when the solidity of the rotor is at the lower limit of about 1-2 %. Should this range be too high, for instance at low wind speeds or high tip speed characteristic, the measured values given here can be matched to the required c_l range by a

---

+) University of Stuttgart, Institute for Aerodynamics and Gas Dynamics

proportionate reduction in camber, without the necessity for making new measurements.

With regard to the behaviour of the blade when stalling, as yet no clear concepts have been developed as to the influence various types of stalling behaviour can have on the controllability and the torsional flutter. For this reason no particular attention is to be paid to this point at first. For the inner section of the blade the airfoil drag is not so important as the ability of the airfoil to develop lift. An airfoil with good lift characteristics can reduce the necessity of providing larger chord lengths at small radii. Since above all structural considerations outweigh all others in this area of the blade, an airfoil is required which is as thick as possible and which possesses good lift properties.

The requirements of the airfoil not only at the outer but also at the inner section of the blade are not usual, and suitable, high-performance airfoils are rarely to be found in the literature [1], [2], [3].

The velocity distributions for two newly-designed airfoils are given in Fig. 1a. The first distribution is for a 15.3% thick airfoil with a pitching moment about the c/4 point of c_m = -.02 and is designed for the outer section of the blade.

The second distribution has a larger pitching moment of c_m = -.07 and supplies a 25.8% thick airfoil for the inner section of the blade.

Figs. 1b and 1c show the speed distributions, as derived from potential theory, for both airfoils at various c_l values. The distribution 258 has been so modified for a third airfoil, that a yet thicker airfoil with 34.3% resulted.

All three airfoils have been build as models for wind tunnel testing and measurements have been carried out by Dipl.-Phys.D.Althaus in the laminar wind tunnel of the Institute at Reynolds numbers from 3 to 5×10^6. Finally the chord length of the 34.3% thick airfoil was shortened by cutting off the airfoil tail, see Fig. 4b, such that the relative airfoil thickness was increased to 40% and with a further cut, up to 50%. Also for these two shortened airfoils (with the designations 400 and 500) $c_l(\alpha)$ graphs and polar diagrams were plotted.

2. Test results

The test results for the five airfoils are shown in Figs. 2 - 6. Fig. 2a contains the $c_l(\alpha)$ graphs for the 15.3% thick airfoil, namely for positive c_l with a smooth airfoil for Re = 3×10^6 and for the rough airfoil for the Reynolds numbers 3, 4 and 5.5×10^6.

By rough it is meant that the transition was triggered off by turbulence wire on both sides of the airfoil close to the leading edge at about 3% of the chord length. The remaining surface of the airfoil remained smooth.

The arrows in the $c_l(\alpha)$ graphs show the area of hysteresis. For negative c_l and Re = 3×10^6 the hysteresis is more marked. A difference between smooth and rough could not here be observed.

Fig. 2a also shows the position of the transition along the chord length as a function of the c_l value. On the abscissa 20° is equivalent to 100% of the chord length. On the lower surface the transition for c_l values above 0.4 migrates quickly to the trailing edge, whereas on the upper surface it migrates only a small amount between 30 - 40% of the chord for all positive c_l. The pitching moment

of this airfoil is about 2-3% for the non-separated flow and changes relatively little even for separated flow.

The model of the second airfoil for wind tunnel testing, with an average thickness of approximately 26-27%, was first of all designed with a trailing edge thickness of 4.2%, which was reduced to 1.66% after the first measurements. It was found that through this the minimum drag values could be reduced from 15×10^{-3} to 8.9×10^{-3}, that is by about 60%. All measurements in Fig. 3a with the model designation 270 S refer to the pointed version shown in Fig. 3b. In the tables of coordinates airfoil 270 S is replaced by airfoil 258 which is practically identical to that measured, but which was designed from the start for a trailing edge thickness of 1%.

Fig. 3a shows the polar diagrams, the $c_l(\alpha)$ and the $c_{m,c/4}(\alpha)$ graphs for the smooth and rough airfoils 270 S.

Exactly in the same way the shapes of the three thick airfoils and the corresponding $c_l(\alpha)$ graphs and polar diagrams are represented in Figs. 4a, 4b and 4c as well as in 5a, 5b and 6a, 6b. For the 34% and the 40% thick airfoils the pitching moments also were measured and for the 40% thick airfoil converted to the c/4 point.

The airfoil thicknesses at the blade roots, which are required for structural reasons, develop remarkably good lift values at moderate drag when the airfoil surfaces are smooth. However the loss of lift when the surface is rough is considerably greater than for thinner airfoils. The high lift/drag ratios in the outer section of the blades are approximately halved by roughness.

The coordinates of the airfoils are given in the tables 1, 2 and 3.

Since also large angles of attack can be of significance for the design of the blade, the lift and drag values of symmetrical and strongly cambered airfoils at two dimensional flow are plotted on the same axes in Figs. 7a and 7b. They can serve as an estimate for the total aerodynamic forces which could possibly occur, but in this case it must be taken into account that the drag values are reduced due to a finite aspect ratio λ. For $\alpha = 90°$ the values must be reduced by approximately the following percentages:

Aspect ratio λ	% Reduction
20	35
30	17
40	10

3. Comparison of various airfoil types

It is often heard that "laminar airfoils" are too sensitive, and that if they were not smooth, they would be less effective than older "standard" airfoils. Such a statement is in general untrue because for smooth surfaces nearly all airfoils are "laminar" and therefore better, and for rough surfaces all airfoils become less effective by the same amount with regard to drag. Refer to Figs. 8 and 9 for an illustration of this (from [2]), in which are represented the "rough" polar diagrams of the airfoils NACA 23012, 4412 as well as 4415. These values are to be compared to the rough polar diagrams of the airfoils proposed in this report.

4. Moment coefficients

The aerodynamic force resulting from lift and drag develops a moment according to the position of the centre of rotation chosen. During wind tunnel testing the centre of rotation in

general lies on the chord of the airfoil at about 25% of the chord length (c/4 point). A clockwise moment has a positive sign. The intersection of the line of action of the aerodynamic force with the airfoil chord is designated as the centre of pressure. The length Δx of the centre of pressure from the centre of rotation is derived from

$$(1) \qquad \frac{\Delta x}{c} = -\frac{dc_m}{dc_l} - \frac{c_{mo}}{c_l} \qquad c = \text{chord length}$$

where c_{mo} is the moment coefficient at $c_l = 0$. ($\Delta x \rightarrow \infty$ represents a counter-clockwise free couple).

Because the aerodynamic force is a combination of the action of the variable blade angle of attack and the fixed blade camber, $\Delta x/c$ is normally not constant for varying angle of attack, but varies mostly between 0 and 0.25. In other words: it can shift between c/4 and c/2 at large and small angles of attack respectively.

For a migrating centre of pressure, however, there exists a so-called neutral point, for which the product of aerodynamic force and a special lever arm, that is the distance between centre of pressure and neutral point, remains constant. In (1) the value dc_m/dc_l goes to zero for the neutral point, and all that remains is the "zero moment" c_{mo}.

The neutral point, which is also often called the aerodynamic centre, is defined by the constancy of the nose-down moment at given dynamic pressure. It is near the c/4 point, for conventional airfoils mostly 2-3% behind this and approximately the same amount beneath the airfoil chord. For symmetrical airfoils without camber the centre of pressure coincides almost with the c/4 point, as long as the flow is not separated. For separated flow it migrates in the direction of c/2. For an S-shaped camber the centre of pressure can

also be fixed in the c/4 point. When centre of pressure and centre of rotation coincide, the aerodynamic moment does not exist. This is, however, a condition of indifferent equilibrium: an alteration of the angle of attack produces no restoring moment.

For static stability (weathervane stability) the centre of rotation must lie in front of the centre of pressure and the c_m (α) graph must take increasingly negative cm values for increasing α . A centre of rotation behind the aerodynamic centre will always be unstable.

If the centre of rotation does not shift on the chord, but normal to this, e.g. due to blade deflection at the wind turbine, the stability can become larger or smaller varying with alterations in angle of attack. This is most easily seen for a symmetrical airfoil: if the centre of rotation lies on the underneath or windward side, then all positive angles of attack will be stable, all negative will be unstable.

If the possibility of free rotation is replaced by the elastic torsional axis of the blade, which usually lies behind the c/4 point, a certain dynamic pressure exists at which the gradient of the distorting moment becomes greater than the gradient of the elastic restoring moment. The blade then suddenly snaps out (divergence). For an untwisted rectangular blade of depth c and span s the corresponding dynamic pressure q is given by:

$$q = \frac{\pi^2 \, G \cdot I}{4 \, \frac{dc_l}{d\alpha} \cdot \frac{\Delta x}{c} \, (c \cdot s)^2} \qquad (2)$$

For airfoils where the centre of pressure hardly moves, for which $\Delta x/c \rightarrow 0$, higher divergence dynamic pressures are more

easily attained than for airfoils with large $\Delta x/c$ for given torsional stiffness G·I. The same tendency is true for the dynamic pressure at which flutter occurs. In addition to this, it is also important for wind turbines to hold the control forces for adjusting the blade small, which also speaks in favour of airfoils with low c_{mo}.

5. Allowable roughness

The surface roughness of an airfoil is a decisive factor for drag and lift of the blade. Roughness can be produced during manufacture of the blade, but can also occur during operation due to icing-up, rain and insects. The essential value is the heigh of roughness K.

For a turbulent boundary layer K should not become larger than the thickness of the so-called viscous sublayer, that is,the following inequality should hold.

$$\frac{v^+ . K}{\nu} < 5 \qquad (3)$$

In this $v^+ = \sqrt{\tau_w/\rho}$ is the skin friction velocity, formed from the shear stress τ_w and density ρ. It is usual to express v^+ by the local frictional coefficient C_f' of the flat plate, where

$$C_f' = \frac{0.059}{Re_x^{0.2}} \qquad (4)$$

(Re_x is the Reynolds number derived from the distance from the leading edge in the downstream direction.) Following from this, with U_∞ as incident flow speed:

$$v^+ = U_\infty \sqrt{\frac{C_f'}{2}}$$

and from equation (3)

$$\frac{U_\infty . K}{\nu} < \frac{7}{\sqrt{C_f'}} \qquad (5)$$

Since with a turbulent boundary layer C_f' varies only slightly with the Reynolds number, Re_x can be approximately set $Re_x = Re_c$ that is, the Reynolds number formed from the local chord length is replaced by that formed from the total chord length. Thus the allowable depth of roughness K results:

Re_t	$\frac{U_\infty K}{\nu}$
10^5	91
10^6	114
10^7	144
10^8	181

In areas of decreasing pressure of an airfoil the allowable K values are almost the same, while in areas of increasing pressure K values approximately 1.2 to 1.4 times as much are permissible.

If the roughness K on a flat plate is double that permitted, the frictional drag increases by about 20%. Should K be five times greater than permissible, the frictional drag increases to 1.5 to 1.7 times that of the smooth plate and becomes independent of the Reynolds number.

Should the height K be referred to the chord length, it can be seen from the table that approximately:

(6) $$\frac{K}{c} \approx \frac{100}{Re_c} \qquad (Re_c \approx 10^6)$$

In Fig. 10 a more exact result is given for the flat plate. It can be seen that, for high values of Reynolds number, the allowable depth of roughness is pretty small, e.g. for $Re_c = 10^7$, $K \approx 10^{-5}\, c$, that is if $c = 5.10^3$ mm, $K = 5.10^{-2}$ mm.

For a laminar boundary layer roughness has a completely different effect: at the critical height of roughness, laminar flow no longer occurs, and a prematurely turbulent boundary layer is produced.

Fig. 10 shows critical depth K for two-dimensional roughnesses, such as turbulence wire. In the laminar case the requirements of surface smoothness are in general less than in the turbulent case and are very much dependent on the distance from the leading edge in the downstream direction. For two-dimensional steps pointing upstream, values of approximately three times as much as in Fig. 10 hold good, whilst steps pointing downstream may have only 1 1/2 times these heights. For three-dimensional "sand" roughnesses approximately double the value in Fig. 10 can be taken as the permissible height.

For surface waviness the relationships are more complicated. Long period single waves should not exceed the given critical K values with regards to their amplitude.

As a first and often remarkably good criterion the human sense of touch can be used. What is registered as "smooth", is generally good enough for a laminar boundary layer.

6. Avoiding roughness

The performance of wind turbines at high tip speed ratios is decisively influenced by the airfoil lift/drag ratio. A smooth surface is therefore important, above all in the outer blade section. Even if the method of manufacture ensures a smooth surface, it can become rough during operation due to rain, insects and icing-up. While rain and ice result in roughness only of short duration, dried-on insects can impair the performance over a very long period. A simple possibility for avoiding insect roughness, and also to reduce the

danger of icing, is to use highly elastic, weather-proof rubber plates about 3-4 mm thick, which are laid around the leading edge. Refer to publication [4].

[1]	Abbott, I.H., A.E.v.Doenhoff	Theory of wing sections. New York, McGraw-Hill 1949
[2]	Riegels, F.W.	Aerodynamische Profile. München, Oldenbourg 1958
[3]	Althaus , D.	"Stuttgarter Profilkatalog I". Stuttgart, Institut für Aerodynamik, 1972
[4]	Wortmann, F.X.	Luftfahrttechnik 9(1963), S.272-274 Schweizer Aero-Revue 38 (1963), Heft 11.

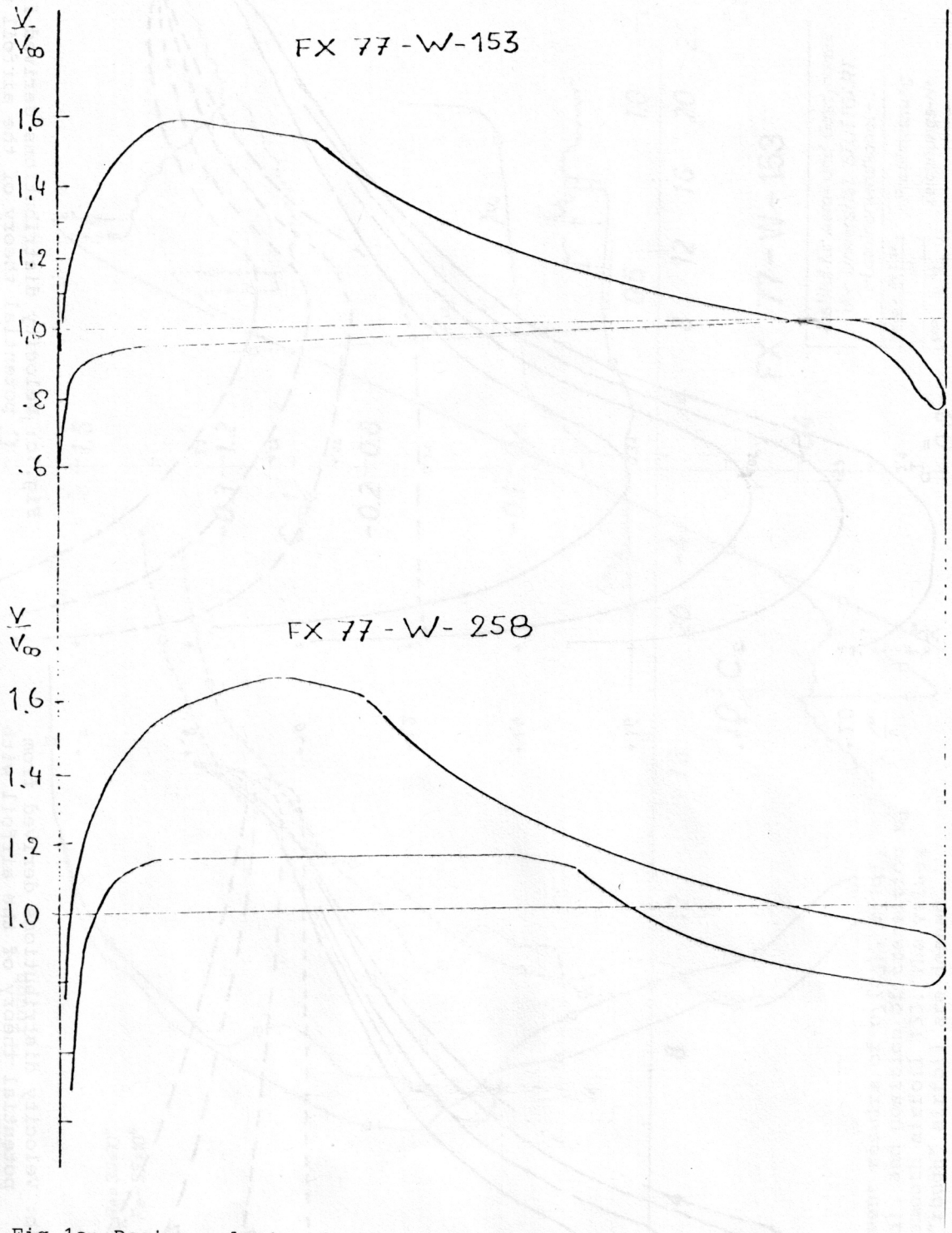

Fig.1a: Design-velocity distribution of the outer section airfoil with 15.3 % thickness and of the inner section airfoil with 25.8 resp.27 % thickness; $c_{li} = 0.7$.

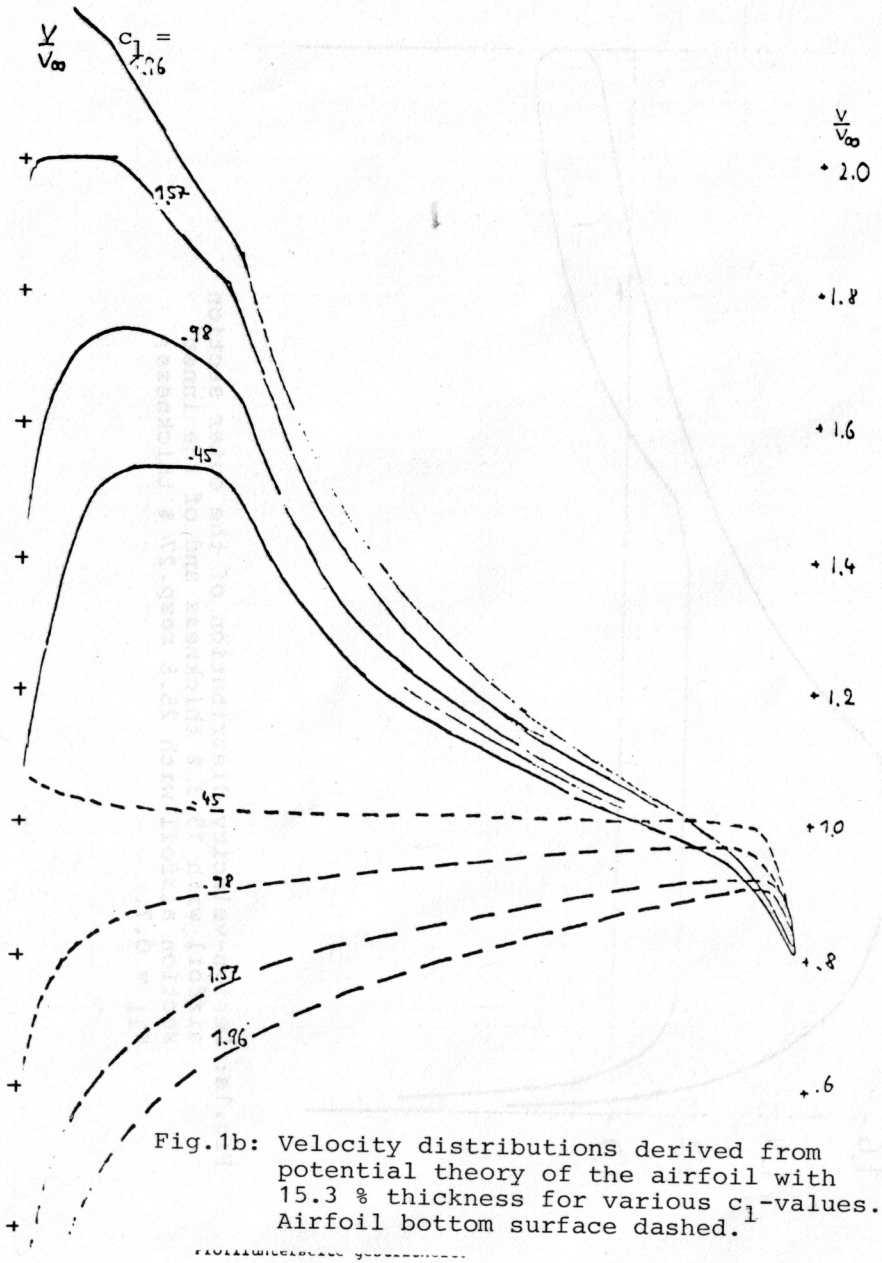

Fig.1b: Velocity distributions derived from potential theory of the airfoil with 15.3 % thickness for various c_l-values. Airfoil bottom surface dashed.

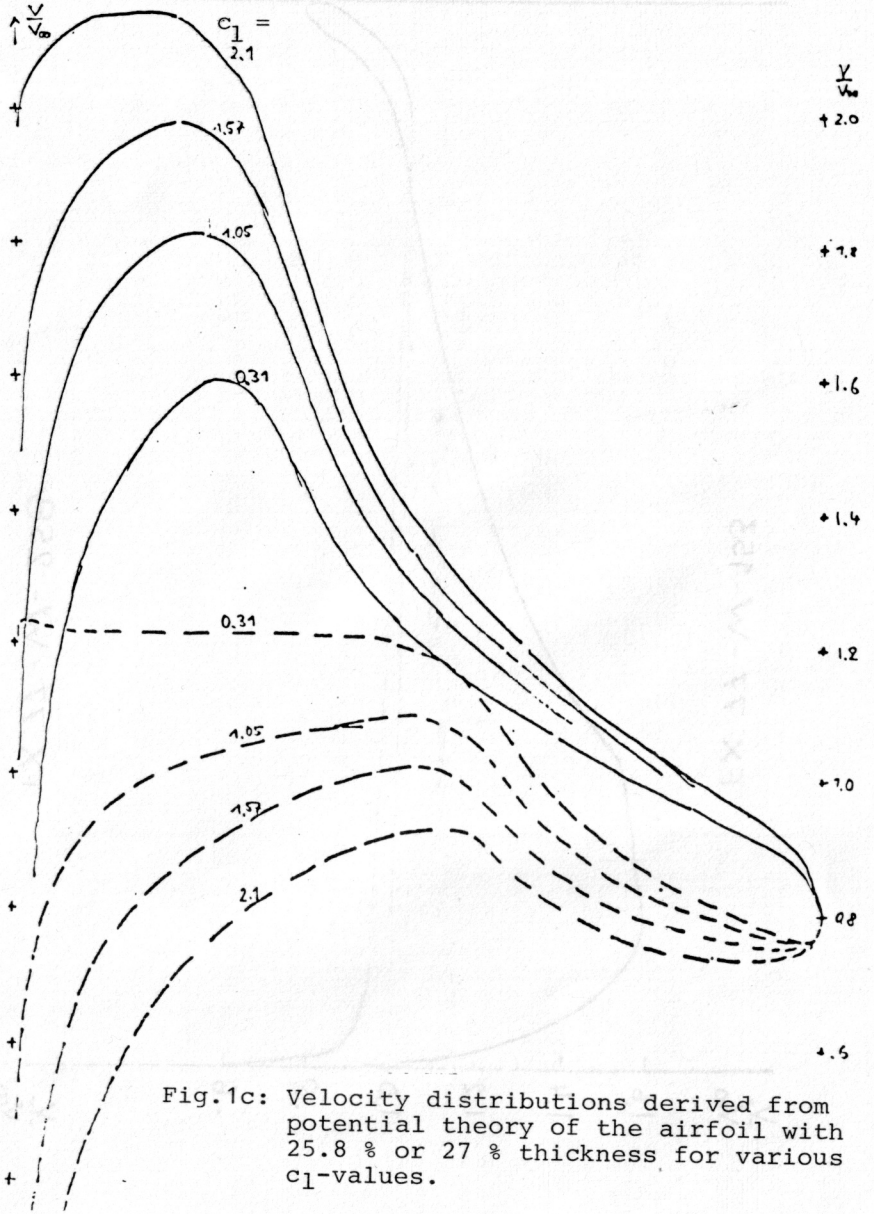

Fig.1c: Velocity distributions derived from potential theory of the airfoil with 25.8 % or 27 % thickness for various c_l-values.

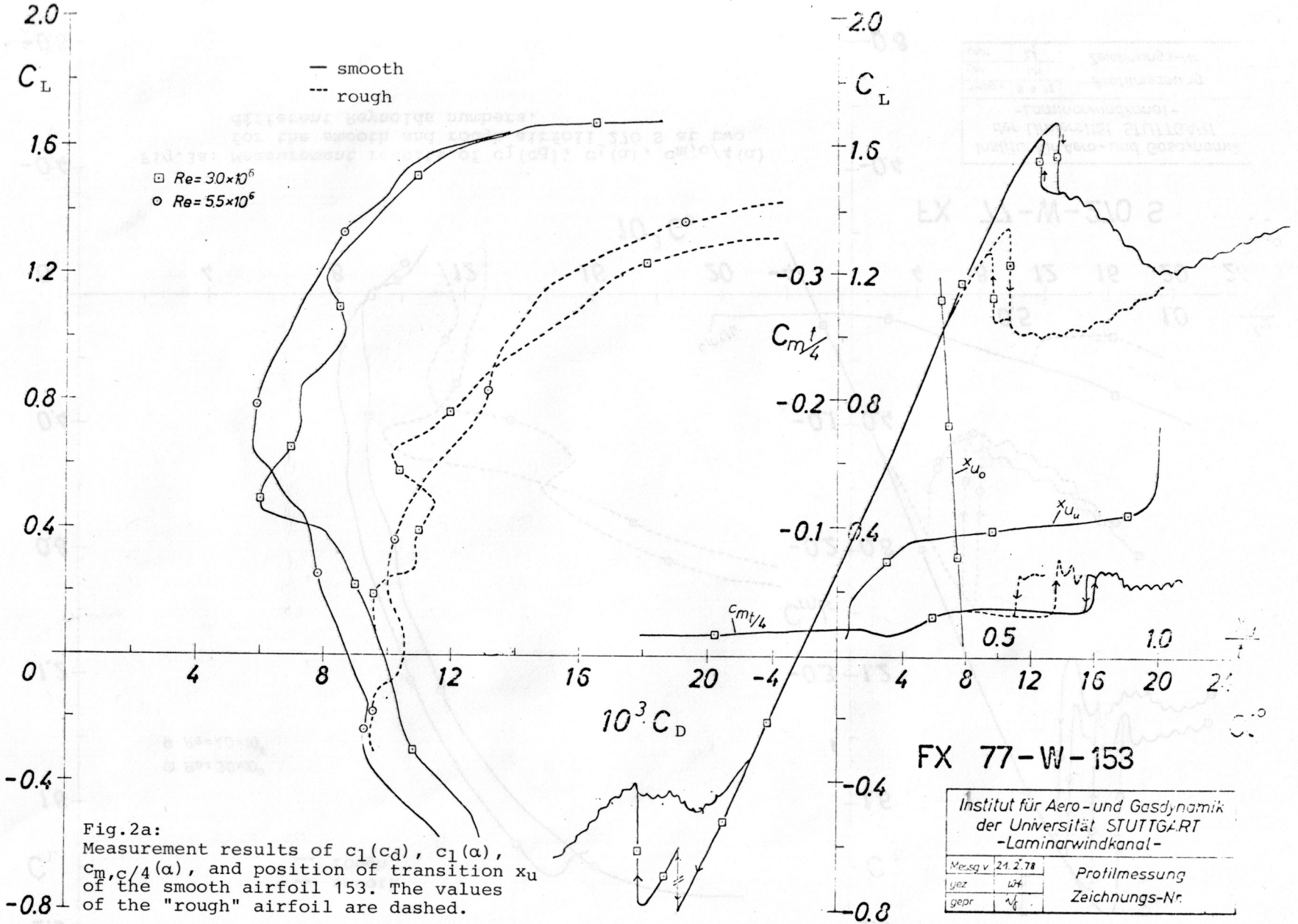

Fig.2a:
Measurement results of $c_l(c_d)$, $c_l(\alpha)$, $c_{m,c/4}(\alpha)$, and position of transition x_u of the smooth airfoil 153. The values of the "rough" airfoil are dashed.

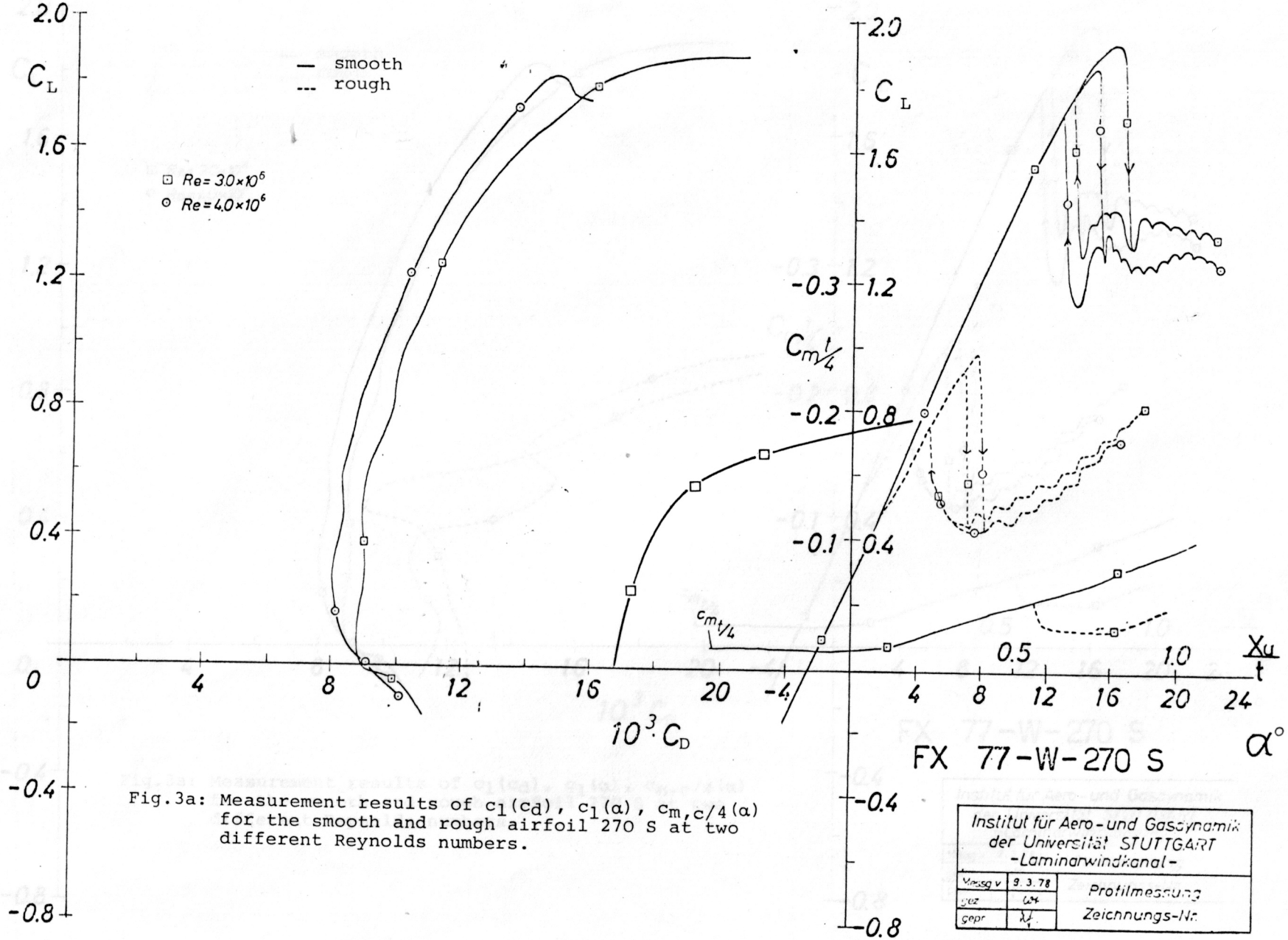

Fig.3a: Measurement results of $c_l(c_d)$, $c_l(\alpha)$, $c_{m,c/4}(\alpha)$ for the smooth and rough airfoil 270 S at two different Reynolds numbers.

Institut für Aero- und Gasdynamik der Universität STUTTGART -Laminarwindkanal-		
Vmessg v	9.3.78	Profilmessung
gez	W.	
gepr	M.	Zeichnungs-Nr.

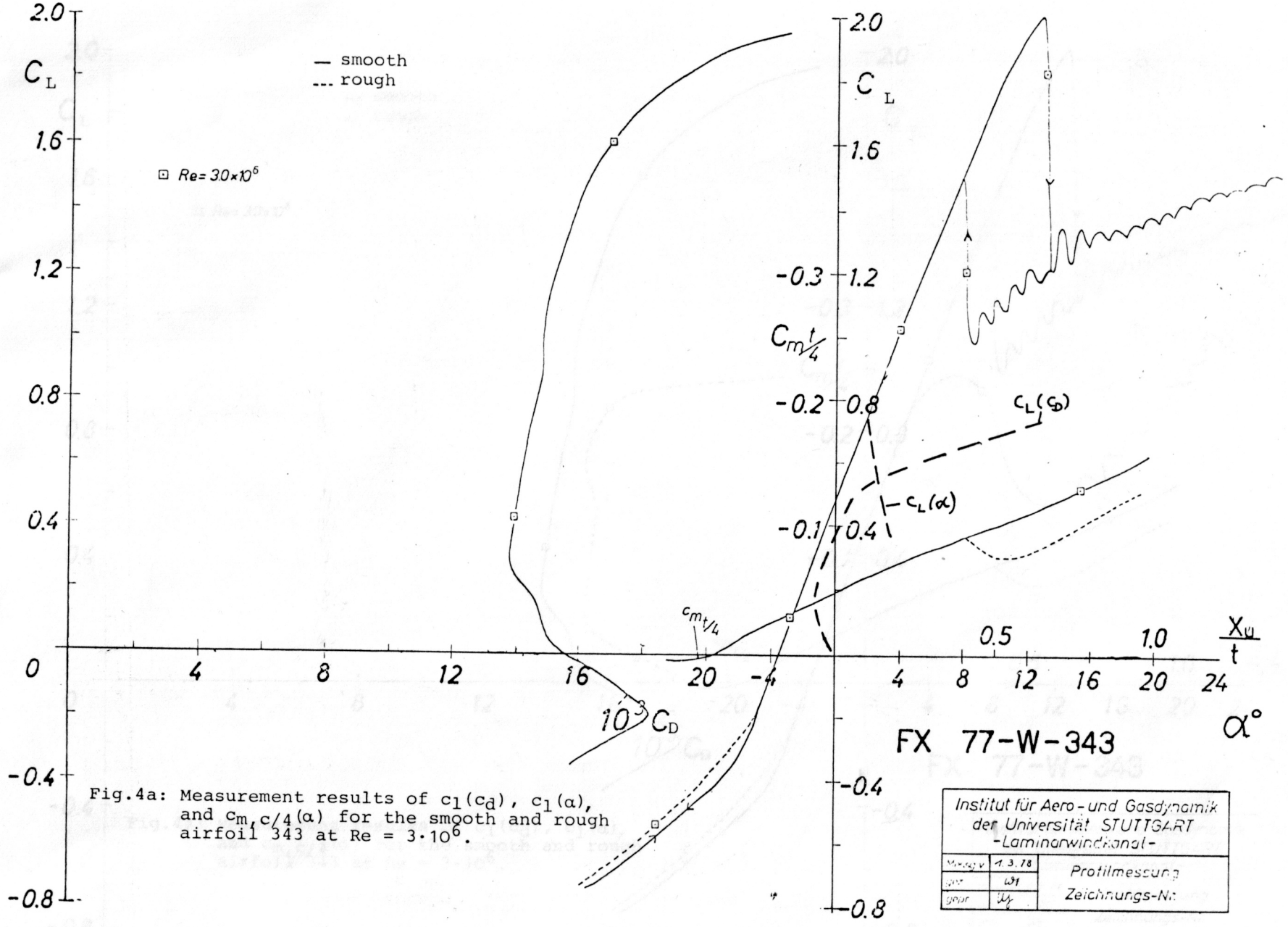

Fig.4a: Measurement results of $c_l(c_d)$, $c_l(\alpha)$, and $c_{m,c/4}(\alpha)$ for the smooth and rough airfoil 343 at Re = $3 \cdot 10^6$.

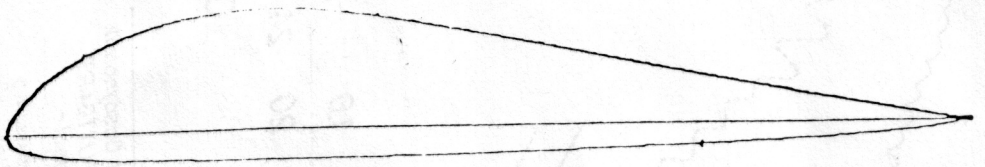

Fig.2b: Contour of the airfoil with 15.3 % thickness

FX 77-W-153

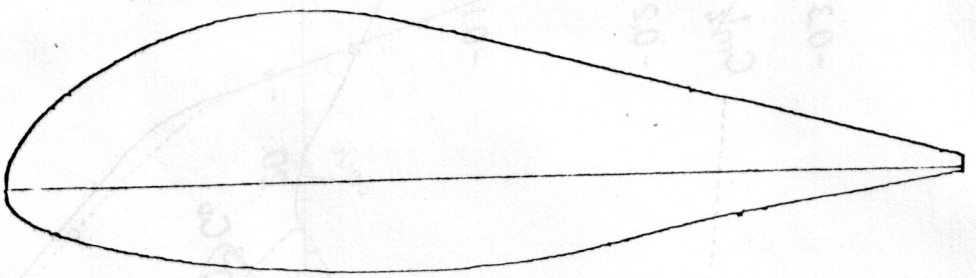

Fig.3b: Contour of the airfoil with 27 % thickness

FX 77-W-270 s

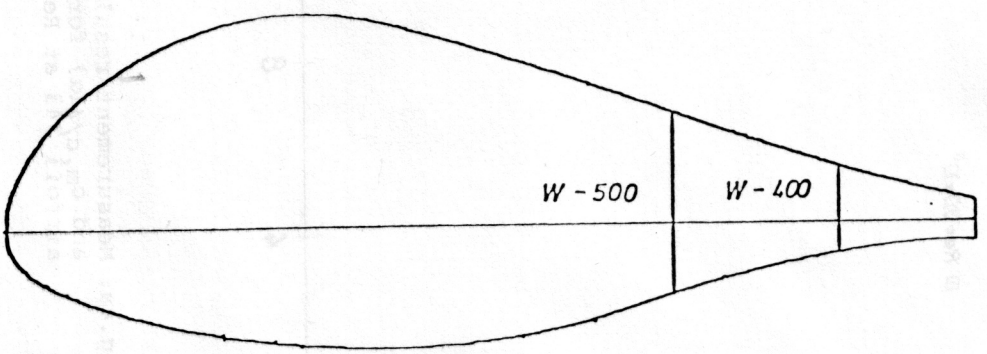

Fig.4b: Contour of the airfoil with 34.3 % thickness as well as of the airfoil 400 and 500.

FX 77-W-343

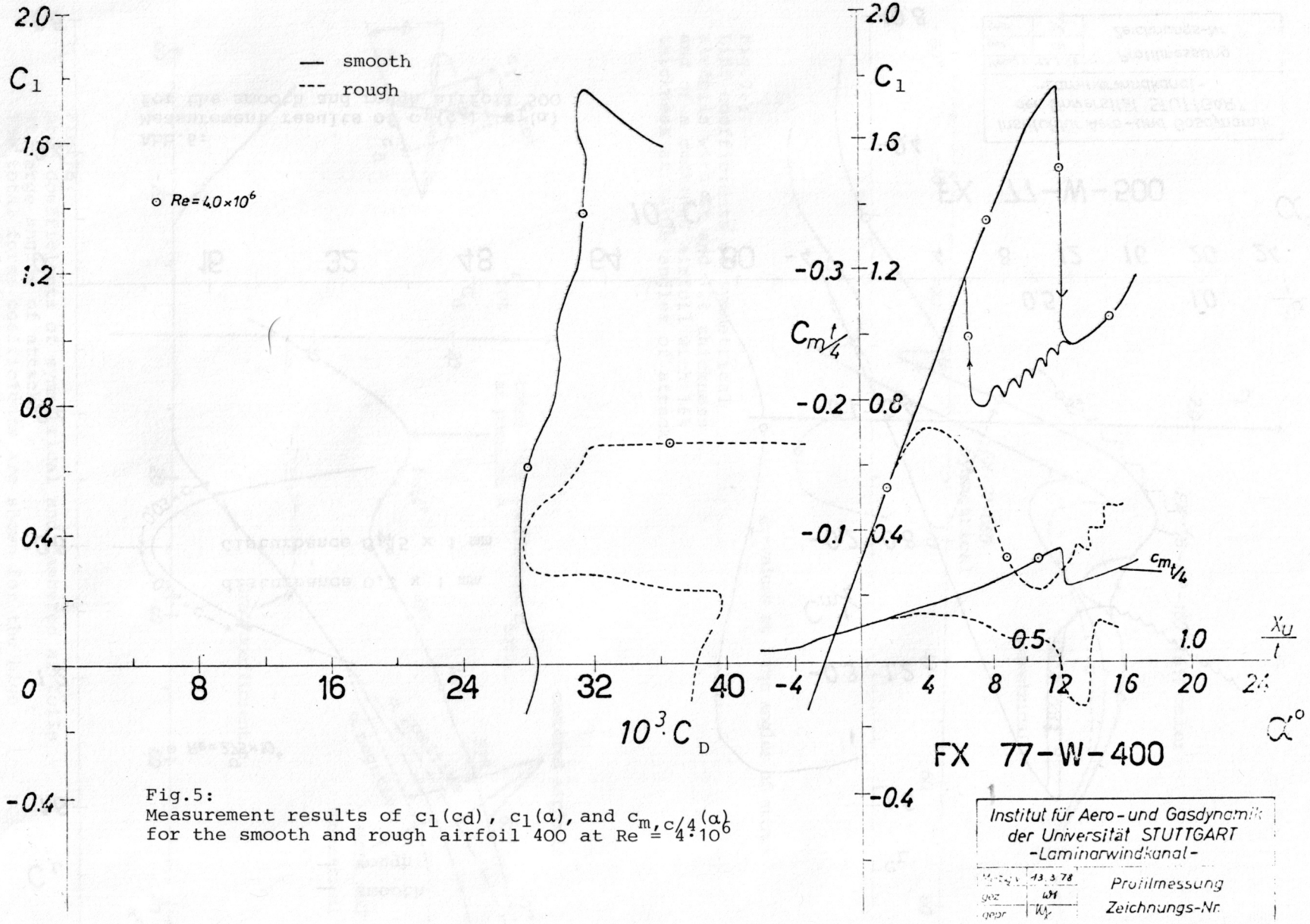

Fig.5:
Measurement results of $c_l(c_d)$, $c_l(\alpha)$, and $c_{m,c/4}(\alpha)$ for the smooth and rough airfoil 400 at $Re = 4 \cdot 10^6$

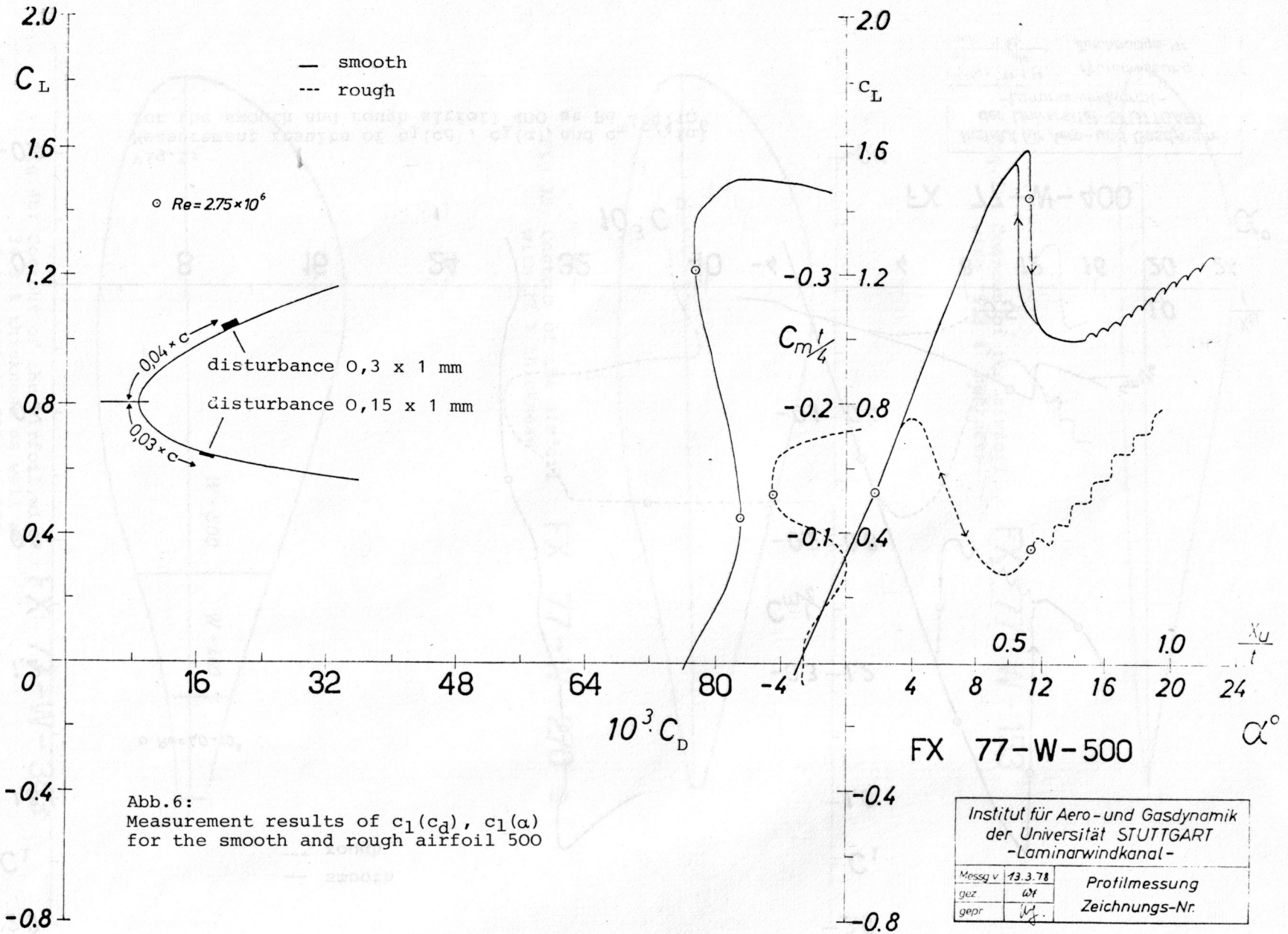

Abb.6:
Measurement results of $c_l(c_d)$, $c_l(\alpha)$
for the smooth and rough airfoil 500

Institut für Aero- und Gasdynamik der Universität STUTTGART -Laminarwindkanal-		
Messg v	13.3.78	Profilmessung
gez		Zeichnungs-Nr.
gepr		

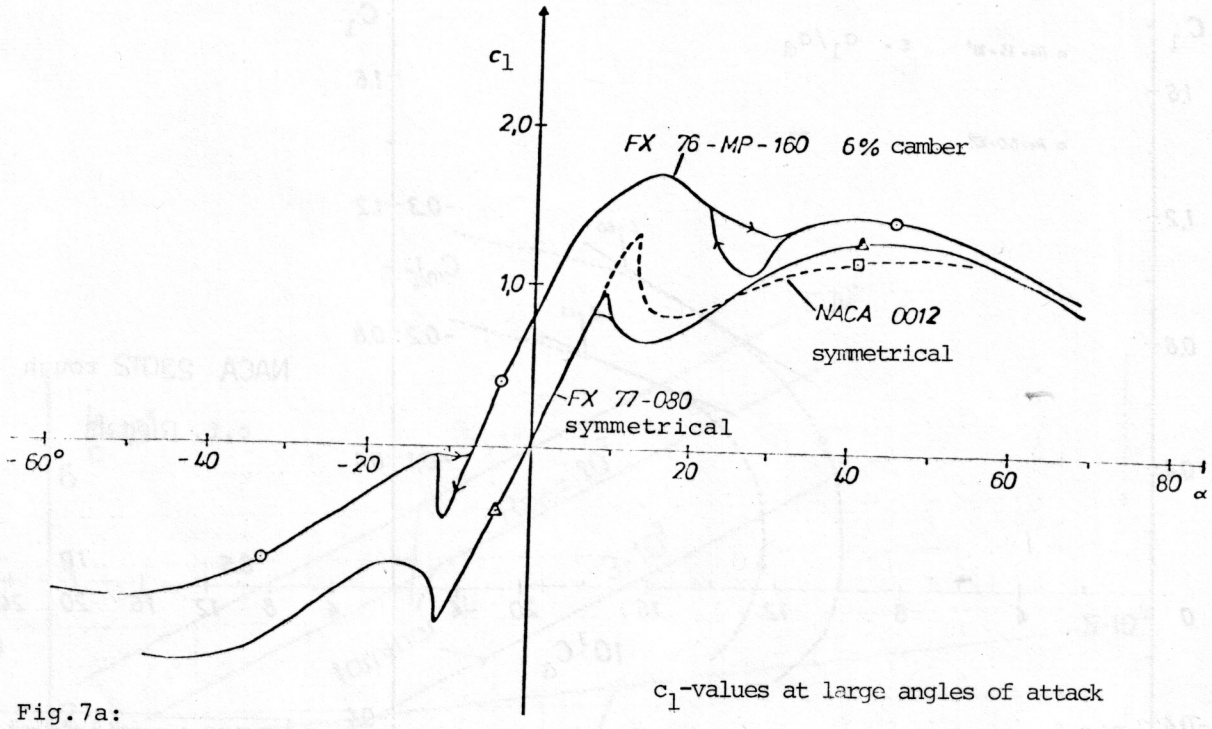

Fig.7a:
Lift coefficients of symmetrical airfoils with 8% and 12% thickness and of a cambered airfoil with 16% thickness at large angles of attack

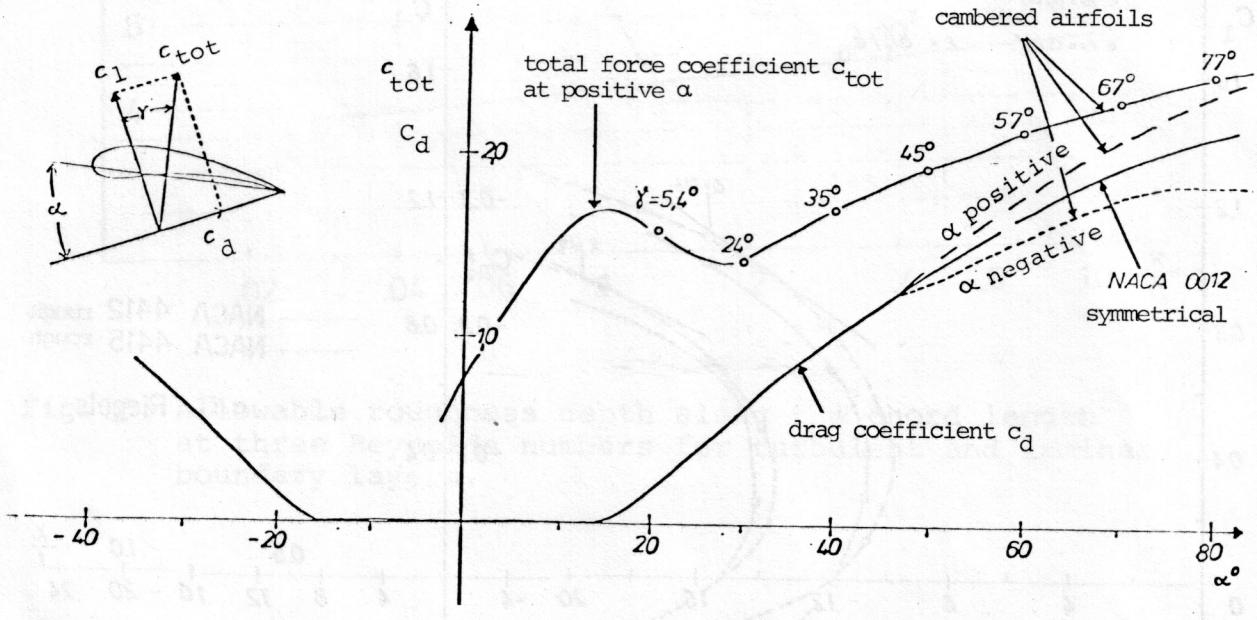

Fig.7b:
Drag coefficients of symmetrical and cambered airfoils at large angles of attack.
The total force coefficients are shown for the high cambered airfoil of Fig.7a.

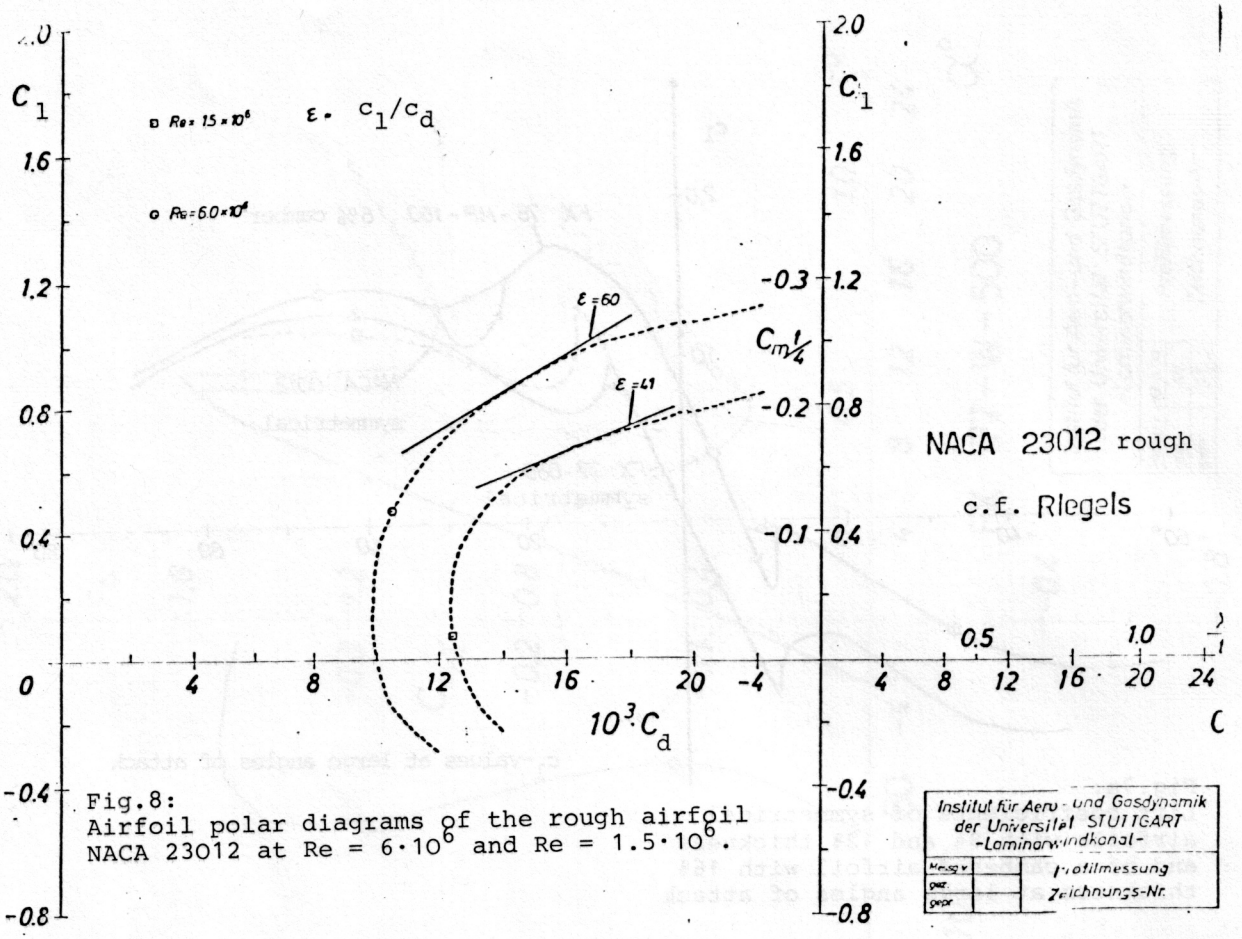

Fig.8:
Airfoil polar diagrams of the rough airfoil NACA 23012 at Re = $6 \cdot 10^6$ and Re = $1.5 \cdot 10^6$.

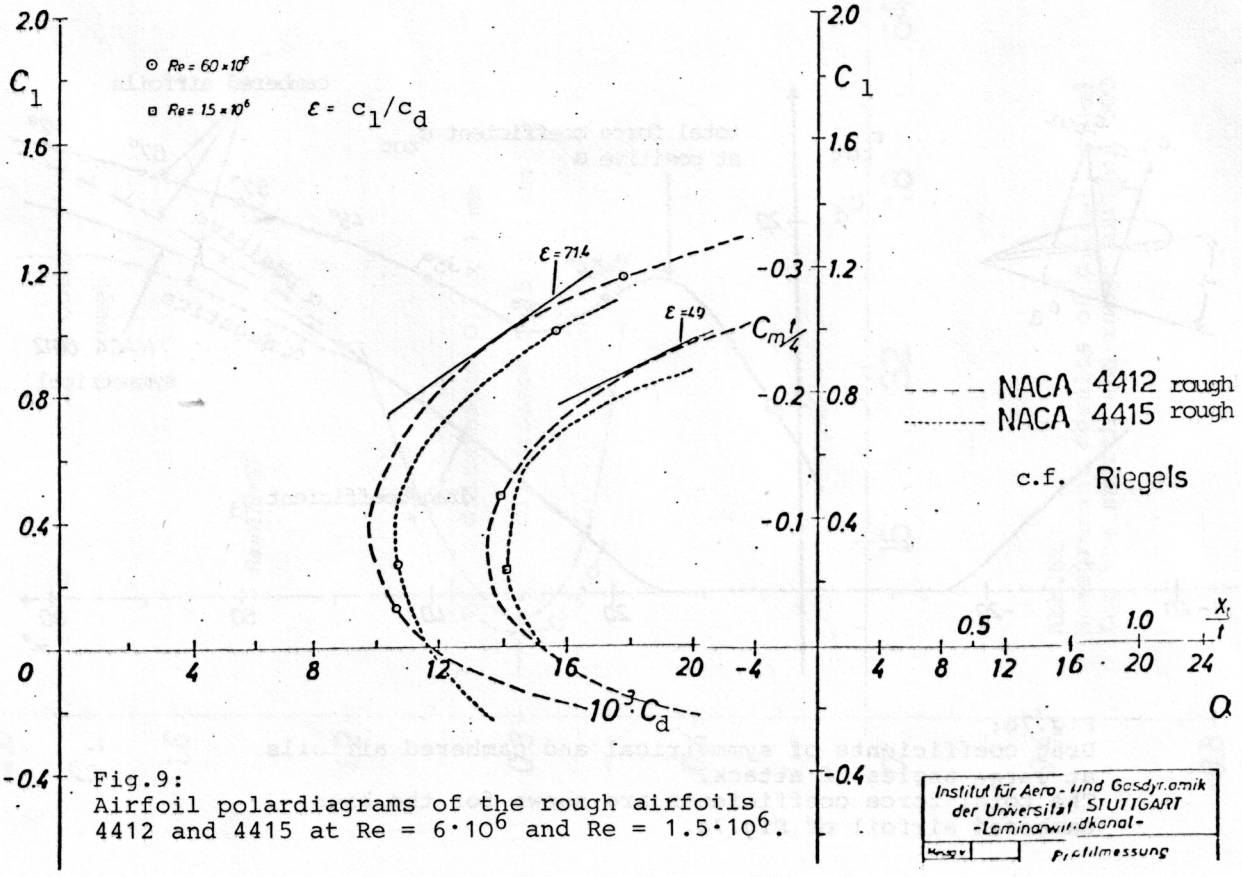

Fig.9:
Airfoil polardiagrams of the rough airfoils 4412 and 4415 at Re = $6 \cdot 10^6$ and Re = $1.5 \cdot 10^6$.

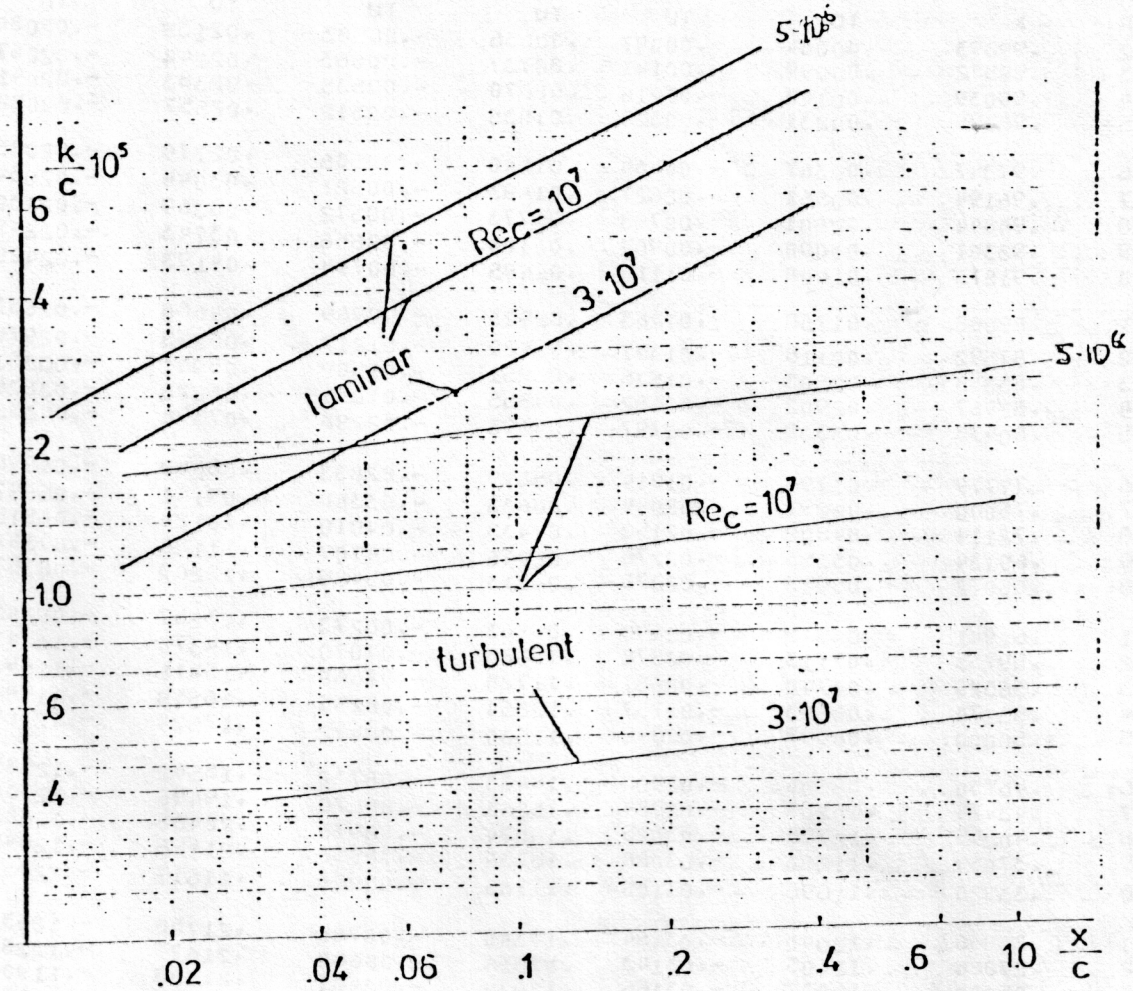

Fig.10: Allowable roughness depth along the chord length at three Reynolds numbers for turbulent and laminar boundary layers.

	List 1			List 2		List 3	
	FX 77-W-153			FX 77-W-258		FX 77-W-343	
NR	X	YO	YU	YO	YU	YO	YU
2	.99893	.00084	-.00097	.00636	-.00583	.02139	-.02084
3	.99572	.00099	-.00141	.00737	-.00563	.02244	-.02067
4	.99039	.00143	-.00216	.00870	-.00535	.02383	-.02041
5	.98296	.00231	-.00325	.01035	-.00512	.02557	-.02022
6	.97347	.00367	-.00464	.01240	-.00506	.02779	-.02025
7	.96194	.00561	-.00627	.01483	-.00521	.03044	-.02054
8	.94844	.00801	-.00793	.01773	-.00572	.03369	-.02130
9	.93301	.01090	-.00962	.02104	-.00656	.03743	-.02245
10	.91573	.01408	-.01115	.02495	-.00794	.04193	-.02429
11	.89668	.01758	-.01263	.02923	-.00969	.04688	-.02657
12	.87592	.02118	-.01397	.03420	-.01217	.05273	-.02979
13	.85355	.02503	-.01536	.03951	-.01509	.05901	-.03353
14	.82967	.02902	-.01662	.04555	-.01891	.06625	-.03828
15	.80438	.03339	-.01797	.05193	-.02298	.07390	-.04356
16	.77779	.03794	-.01914	.05899	-.02803	.08248	-.04996
17	.75000	.04291	-.02044	.06633	-.03360	.09141	-.05697
18	.72114	.04802	-.02152	.07433	-.04010	.10124	-.06515
19	.69134	.05355	-.02276	.08246	-.04707	.11126	-.07387
20	.66072	.05913	-.02376	.09113	-.05489	.12203	-.08367
21	.62941	.06512	-.02490	.09963	-.06273	.13257	-.09343
22	.59755	.07113	-.02578	.10863	-.07070	.14370	-.10343
23	.56526	.07740	-.02681	.11728	-.07660	.15411	-.11093
24	.53270	.08363	-.02757	.12654	-.08155	.16510	-.11741
25	.50000	.08997	-.02846	.13530	-.08472	.17524	-.12169
26	.46730	.09606	-.02908	.14433	-.08732	.18562	-.12533
27	.43474	.10209	-.02984	.15263	-.08870	.19496	-.12738
28	.40245	.10758	-.03025	.16074	-.08970	.20408	-.12883
29	.37059	.11280	-.03088	.16730	-.08958	.21126	-.12843
30	.33928	.11696	-.03105	.17185	-.08920	.21617	-.12758
31	.30866	.12040	-.03154	.17540	-.08785	.21750	-.12531
32	.27886	.12105	-.03143	.17516	-.08640	.21677	-.12282
33	.25000	.12037	-.03166	.17039	-.08401	.21303	-.11906
34	.22221	.11791	-.03134	.16616	-.08163	.20757	-.11521
35	.19562	.11449	-.03123	.15975	-.07832	.19952	-.11019
36	.17033	.10954	-.03064	.15241	-.07517	.19034	-.10527
37	.14645	.10372	-.03021	.14329	-.07104	.17903	-.09919
38	.12408	.09639	-.02929	.13370	-.06724	.16710	-.09344
39	.10332	.08836	-.02849	.12248	-.06239	.15320	-.08650
40	.08427	.07928	-.02713	.11134	-.05803	.13928	-.08013
41	.06699	.07013	-.02598	.09689	-.05261	.12379	-.07250
42	.05156	.06014	-.02414	.08696	-.04787	.10884	-.06587
43	.03806	.05048	-.02255	.07397	-.04193	.09267	-.05777
44	.02653	.04032	-.02016	.06221	-.03699	.07799	-.05081
45	.01704	.03089	-.01817	.04961	-.03070	.06240	-.04218
46	.00961	.02143	-.01482	.03902	-.02524	.04911	-.03430
47	.00428	.01365	-.01115	.02722	-.01764	.03419	-.02386
48	.00107	.00591	-.00464	.01752	-.01273	.02141	-.01624